



**HAL**  
open science

## Spectrin-like repeats 11-15 of human dystrophin show adaptations to a lipidic environment.

Joe Sarkis, Jean-François Hubert, Baptiste Legrand, Estelle Robert, Angélique Chéron, Julien Jardin, Eric Hitti, Elisabeth Le Rumeur, Véronique Vié

### ► To cite this version:

Joe Sarkis, Jean-François Hubert, Baptiste Legrand, Estelle Robert, Angélique Chéron, et al.. Spectrin-like repeats 11-15 of human dystrophin show adaptations to a lipidic environment.. *Journal of Biological Chemistry*, 2011, 286 (35), pp.30481-91. 10.1074/jbc.M111.243881 . inserm-00712828

**HAL Id: inserm-00712828**

**<https://inserm.hal.science/inserm-00712828>**

Submitted on 29 May 2020

**HAL** is a multi-disciplinary open access archive for the deposit and dissemination of scientific research documents, whether they are published or not. The documents may come from teaching and research institutions in France or abroad, or from public or private research centers.

L'archive ouverte pluridisciplinaire **HAL**, est destinée au dépôt et à la diffusion de documents scientifiques de niveau recherche, publiés ou non, émanant des établissements d'enseignement et de recherche français ou étrangers, des laboratoires publics ou privés.

Copyright

# Spectrin-like Repeats 11–15 of Human Dystrophin Show Adaptations to a Lipidic Environment<sup>\*[5]</sup>

Received for publication, March 25, 2011, and in revised form, June 24, 2011. Published, JBC Papers in Press, June 28, 2011, DOI 10.1074/jbc.M111.243881

Joe Sarkis<sup>‡§¶1</sup>, Jean-François Hubert<sup>‡§</sup>, Baptiste Legrand<sup>‡§</sup>, Estelle Robert<sup>‡¶</sup>, Angélique Chéron<sup>‡§</sup>, Julien Jardin<sup>¶||</sup>, Eric Hitti<sup>‡\*\*\*</sup>, Elisabeth Le Rumeur<sup>‡§</sup>, and Véronique Vie<sup>‡¶12</sup>

From the <sup>‡</sup>Université Européenne de Bretagne, 35000 Rennes, France, <sup>§</sup>UMR-CNRS 6026-IFR 140, Equipe RMN-Interactions Lipides Protéines, Faculté de Médecine, CS 34317, 35043 Rennes, France, and <sup>¶</sup>UMR-CNRS 6251, Institut de Physique de Rennes, Université de Rennes 1, 35042 Rennes, France, the <sup>||</sup>Institut National de la Recherche Agronomique (INRA), AGROCAMPUS-OUEST, UMR 1253, Science et Technologie du Lait et de l'Oeuf, 35042 Rennes, France, and the <sup>\*\*</sup>Laboratoire Traitement du Signal et de l'Image (LTSI), INSERM 642, 35042 Rennes, France

Dystrophin is essential to skeletal muscle function and confers resistance to the sarcolemma by interacting with cytoskeleton and membrane. In the present work, we characterized the behavior of dystrophin 11–15 (DYS R11–15), five spectrin-like repeats from the central domain of human dystrophin, with lipids. DYS R11–15 displays an amphiphilic character at the liquid/air interface while maintaining its secondary  $\alpha$ -helical structure. The interaction of DYS R11–15 with small unilamellar vesicles (SUVs) depends on the lipid nature, which is not the case with large unilamellar vesicles (LUVs). In addition, switching from anionic SUVs to anionic LUVs suggests the lipid packing as a crucial factor for the interaction of protein and lipid. The monolayer model and the modulation of surface pressure aim to mimic the muscle at work (*i.e.* dynamic changes of muscle membrane during contraction and relaxation) (high and low surface pressure). Strikingly, the lateral pressure modifies the protein organization. Increasing the lateral pressure leads the proteins to be organized in a regular network. Nevertheless, a different protein conformation after its binding to monolayer is revealed by trypsin proteolysis. Label-free quantification by nano-LC/MS/MS allowed identification of the helices in repeats 12 and 13 involved in the interaction with anionic SUVs. These results, combined with our previous studies, indicate that DYS R11–15 constitutes the only part of dystrophin that interacts with anionic as well as zwitterionic lipids and adapts its interaction and organization depending on lipid packing and lipid nature. We provide strong experimental evidence for a physiological role of the central domain of dystrophin in sarcolemma scaffolding through modulation of lipid-protein interactions.

Dystrophin is a rod-shaped cytoplasmic protein that constitutes a vital part of a protein complex that connects the cytoskeleton of muscle fibers to the surrounding extracellular matrix through the cell membrane. This long, filamentous pro-

tein (Fig. 1A) is essential to skeletal muscle function, which is demonstrated by the lethal pathophysiology associated with its deficiency, namely Duchenne muscular dystrophy (1). Several membrane and cytoskeletal binding partners of dystrophin have been identified, including  $\beta$ -dystroglycan from the dystrophin-glycoprotein complex (2, 3).  $\beta$ -Dystroglycan interacts with the cysteine-rich region of dystrophin that is located between the stabilizing central domain, which consists of 24 spectrin-like repeats and is known as the rod domain, and the C-terminal end of the molecule. Cytoskeletal actin interacts with the dystrophin molecule through two actin-binding domains, ABD1 and ABD2, which are situated at the N-terminal end and at the center of the dystrophin rod domain (repeats 11–15), respectively (4). The subsarcolemmal location of dystrophin and its association with both the cytoskeleton and membrane suggest a role in the mechanical regulation of membrane stress during contraction and elongation of muscle fibers at work (5), when bending, blebbing, and various levels of packing occur. In particular, phenotype rescues of Duchenne muscular dystrophy mouse models have shown that some parts of the rod domain of dystrophin are essential for dystrophin function (6). We recently reviewed dystrophin function (7) and concluded that although little is known about the mechanisms that trigger dystrophy disease at the molecular level, the rod domain of dystrophin is no longer considered to be a passive linker; rather, it is thought to have a key role in regulating the membrane cytoskeleton and the extracellular matrix scaffold. Nevertheless, many aspects of rod domain structure and function are still unknown, and it is of great interest to map the entire protein for binding domains and mechanical properties, particularly those linked to membrane. Our previous studies have shown that DYS R1–3<sup>3</sup> strongly interacts with small unilamellar vesicles (SUVs), whereas DYS R20–24 displays very weak lipid binding properties (8, 9). In addition, repeats 1–3 and 4–19 are able to bind to anionic lipids and represent two lipid

\* This work was supported by the "Association Française contre les Myopathies" and by RTR-BRESMAT (Université Européenne de Bretagne).

[5] The on-line version of this article (available at <http://www.jbc.org>) contains supplemental Figs. S1–S4.

<sup>1</sup> Recipient of a doctoral fellowship from the French Minister of Research.

<sup>2</sup> To whom correspondence should be addressed: 263 Av. Général Leclerc, Institut de Physique de Rennes, UMR CNRS 6251-Bât 11 A, 35042 Rennes Cedex, France. Tel.: 33-2-23-23-56-45; E-mail: veronique.vie@univ-rennes1.fr.

<sup>3</sup> The abbreviations used are: DYS R1–3, DYS R11–15, and DYS20–24, subdomain comprising human dystrophin repeats 1–3, 11–15, and 20–24, respectively; SUV, small unilamellar vesicle; LUV, large unilamellar vesicle; DOPC, 1,2-dioleoyl-*sn*-glycero-3-phosphocholine; DOPS, 1,2-dioleoyl-*sn*-glycero-3-phospho-L-serine; DOPE, 1,2-dioleoyl-*sn*-glycero-3-phosphoethanolamine; mN, millinewtons; AFM, atomic force microscopy; HA, HB, and HC, helix A, B, and C, respectively; PM-IRRAS, polarization modulation infrared reflection adsorption spectroscopy.

TABLE 1

## Human dystrophin rod 11–15 subdomain construct

Residues in boldface type indicate the start (N terminus column) or end (C terminus column) residue of the repeat from the alignment of Winder *et al.* (13). Underlined residues indicate the start (N terminus column) or end (C terminus column) residue of the repeat from the alignment of Koenig and Kunkel (57). GS, residues left at the N terminus after cleavage of the tags.

Construct (number of residues)	Start residue	End residue	N terminus	C terminus
DYS R11–15 (515) <sup>a</sup>	1461	1973	<u>GS</u> FQK <u>PAN</u> ...	...RLNFAQ

<sup>a</sup> The DYS R11–15 (residues 1–515) protein used in this study corresponds to residues 1461–1973 of native full-length dystrophin.

binding domains, called LBD1 and LBD2 (7, 10), respectively. The lipid-binding properties of the rod domain are probably required to provide mechanical stability to the sarcolemma, as shown in the case of the spectrin-related cytoskeleton of the erythrocyte (11). Among the repeats and subdomains that have been previously studied, DYS R11–15 corresponds to a unique region of the dystrophin rod domain that is rich in basic amino acids and interacts with anionic membrane lipids. In contrast with other repeats, this domain exhibits slight tryptophan fluorescence quenching when in contact with zwitterionic SUVs, which suggests a binding interaction with these lipids (10). The region DYS R11–15 has also been reported as a second actin-binding domain (ABD2) (4) in dystrophin. These five repeats are part of the rod domain that may constitute a direct link between the sarcolemma and cytoskeleton. It is of great interest to characterize the behavior of these repeats in order to understand the adaptation mechanisms of cell muscle membranes to mechanical stress. To investigate the impacts of lipid packing and lipid composition on DYS R11–15 function, we characterized the interaction and the organization of DYS R11–15 with two lipid mixtures, 1,2-dioleoyl-*sn*-glycero-3-phosphocholine/1,2-dioleoyl-*sn*-glycero-3-phospho-L-serine (DOPC/DOPS) (1:1) and 1,2-dioleoyl-*sn*-glycero-3-phosphocholine:1,2-dioleoyl-*sn*-glycero-3-phosphoethanolamine (DOPC/DOPE) (1/1), in vesicles (SUVs and LUVs) and monolayer lipid membrane models. These lipids were chosen because of their presence in the sarcolemma (12), where DO fatty acids constitute 12% of the global membrane composition. We used DOPC/DOPS or DOPC/DOPE lipid mixtures at a 1:1 ratio (mol/mol) because phosphatidylcholine represents ~45%, phosphatidylethanolamine 23%, and phosphatidylserine 18% of the total phospholipids and to enhance potential specific effects of phosphatidylethanolamine compared with PS.

## EXPERIMENTAL PROCEDURES

## Materials

All lipids were obtained from Avanti Polar Lipids (Alabaster, AL) and were used without further purification. The pGEX-4T1 plasmid vector and a GST-Trap<sup>TM</sup> HP column were purchased from GE Healthcare. Ozyme (St. Quentin-en-Yvelines, France) supplied the ER2566 bacteria and restriction enzymes. Sequencing grade trypsin was from Promega.

## Protein Expression and Purification

Protein constructs were designed as described in Table 1. The boundaries of the DYS R11–15 protein were chosen without any extension based on the original alignment described by Winder *et al.* (13). DYS R11–15, R1–3, and R20–24 were expressed as GST-tagged proteins in *Escherichia coli* and were purified as described previously (10). Purity was assessed by

SDS-PAGE with Coomassie Blue staining, and protein concentrations were determined using the bicinchoninic acid protein assay (14).

## Phospholipid Vesicle Preparations

Multilamellar vesicles were prepared first. Mixtures containing one part DOPC to one part DOPS or DOPE (mol/mol) in chloroform were dried overnight under vacuum and were suspended in 150 mM NaCl and 0.1 mM EDTA buffered with 100 mM Tris-HCl at pH 7.5 (TNE buffer). SUVs with a mean diameter of 30 nm were prepared from multilamellar vesicles diluted to 25 mg of lipid/ml and sonicated at 4 °C (U200S, UKA Labortechnik) for 2 min with half-duty cycles. Oxidation products were not detected in the SUVs obtained after sonication (15). The sizes of the SUVs and LUVs were verified by dynamic light scattering (4700/PCS100 spectrometer, Malvern) and electron microscopy (JEOL 100 CX).

## DYS R11–15 and Liposome Interactions

*Steady-state Fluorescence Measurements*—Steady-state fluorescence measurements were performed by adding 0.5 μM DYS R11–15 in TNE buffer to liposomes at different concentrations to achieve a final volume of 300 μl. Tryptophan fluorescence emission spectra were recorded between 310 and 420 nm using an excitation wavelength of 295 nm (bandwidth, 2 nm) on a Fluorolog spectrofluorometer (Jobin-Yvon, Longjumeau, France) using 10 × 2-mm quartz cuvettes at 20 °C.

*Proteolytic Digestions on Vesicles*—Samples containing 0.5 μM DYS R11–15 alone, with 0.5 mM SUVs (30 nm), and with 0.5 mM LUVs (100, 200, and 400 nm) were incubated for 2 h at room temperature in TNE buffer. SUVs and LUVs were generated with a DOPC/DOPS or DOPC/DOPE lipid mixture. Samples were incubated with 200 μg/ml trypsin. Aliquots were removed at different time intervals after the addition of the protease and transferred into Laemmli denaturing buffer. Samples were visualized using 15% SDS-PAGE stained by silver nitrate.

## DYS R11–15/Langmuir Experiments

Before the experiments were begun, small circular Teflon troughs with subphase volumes of 3 or 8 ml were cleaned with ethanol and water and filled with TNE buffer. All experiments were performed between 19 and 21 °C.

*Air/Liquid Interface Measurements*—The experiments in the absence of lipid at the air/liquid interface, prior to lipid/liquid interface, allow determination of the following: (i) the amphiphilic properties of the protein; (ii) the concentration at which the protein saturates the lipid-free interface (16) in a way to minimize the protein aggregation that could result from a high protein concentration; and (iii) the concentration of the protein

that will be used in the experiments with lipids. In these studies, this concentration is usually chosen slightly lower than the concentration of saturation (16–18). The protein was injected into the subphase solution at final concentrations ranging from 0.01 to 1  $\mu\text{M}$ . The surface pressure was recorded continuously until it stabilized. Each experiment was repeated at least three times, and the  $\pi$  values were found to be reproducible to within  $\pm 0.3$  mN/m.

*In situ* infrared spectroscopy was used to study the stability and the secondary structure of the protein at the air/liquid interface. The PM-IRRAS spectra were recorded on a Nicolet 870 FT-IR spectrometer (Thermo Electron, Madison, WI). PM-IRRAS combines Fourier transform infrared reflection spectroscopy of an interface with fast modulation of the polarization of the infrared radiation between parallel ( $p$ ) and perpendicular ( $s$ ) directions with respect to the plane of incidence (19, 20). The FT is calculated with data points every 1  $\text{cm}^{-1}$  with a final spectral resolution of 8  $\text{cm}^{-1}$  by co-adding 2400 scans. The details of the optical setup, experimental procedure, and two-channel processing of the detected intensity have been described previously (20). The PM-IRRAS spectra were acquired over several time intervals while the surface pressure stabilized and are displayed after the water bands were subtracted from the subphase (TNE buffer) spectrum.

*Lipid/Liquid Interface Measurements*—Monolayer films have become a standard model for studying lipid-protein interactions and associations in biological membranes (21). Lipid mixtures (DOPC/DOPS and DOPC/DOPE) in a 2:1 chloroform/methanol solution (v/v) were gently spread at the air/liquid interface of the TNE buffer subphase in the 8-ml circular Teflon trough at the desired surface pressure, which ranges from 15 to 32 mN/m. This surface pressure is called the initial lipid surface pressure ( $\pi_i$ ). The protein was injected into the subphase just beneath the lipid monolayer at a final concentration of 0.1  $\mu\text{M}$ . The increased surface pressure and ellipsometric angle due to adsorption of the protein to the monolayer were recorded continuously as functions of time.

*Surface Pressure and Ellipsometry*—The ellipsometric angle ( $\Delta$ ) and surface pressure ( $\pi$ ) in the trough were recorded simultaneously. The surface pressure was measured using the Wilhelmy method (Nima Technology, Cambridge, UK). The ellipsometric measurements were carried out with a conventional null ellipsometer using a helium-neon laser operating at 632.8 nm. In this “null ellipsometer” configuration (22), the analyzer angle, multiplied by 2, yielded the value of the ellipsometric angle  $\Delta$ . Variations in the ellipsometric angle are related to the phase difference between the parallel and perpendicular polarizations of the reflected light. The procedure is described elsewhere (23).

*Atomic Force Microscopy*—A computer-controlled and user-programmable Langmuir trough (Nima Technology) equipped with two movable barriers was used to measure the surface pressure and prepare AFM samples. Imaging samples were obtained using the Langmuir-Blodgett technique. The process requires a slow vertically lifting of the slides from the subphase to air, termed Blodgett deposition (24, 25), and is usually associated with AFM to characterize molecular organization of the monolayer. After the surface pressure stabilized, the Langmuir film was transferred to freshly cleaved mica plates at constant surface pressure by vertically raising (1 mm/min) the mica

through the lipid/liquid interface. In some cases, 200  $\mu\text{g/ml}$  trypsin was injected into the subphase 20 min or 2 h before the Langmuir-Blodgett transfer. AFM imaging of Langmuir-Blodgett films was performed in contact mode using a Pico-plus atomic force microscope (Agilent Technologies, Phoenix, AZ) under ambient conditions with a scanning area of  $10 \times 10 \mu\text{m}^2$ . Topographic images were acquired in constant force mode using silicon nitride tips on integral cantilevers with a nominal spring constant of 0.06 newtons/m. Representative images were obtained from at least two samples prepared on different days and from at least five macroscopically separated areas on each sample.

### Identification of Peptides by Nano-LC/MS/MS

Samples containing DYS R11–15 alone or in the presence of SUVs in a 1:1000 (mol/mol) ratio were prepared. Trypsin was added to a final concentration of 0.1 g/liter. After 20 min, digestion was stopped by adding 0.2% trifluoroacetic acid (TFA) (Pierce), and the samples were analyzed by tandem mass spectrometry (MS/MS). All mass spectra were measured using a hybrid quadrupole TOF mass spectrometer QStar XL (MDS Sciex, Toronto, Canada). The instrument was calibrated with a multipoint calibration that used fragment ions resulting from collision-induced decomposition of a peptide from  $\beta$ -casein,  $\beta$ -CN(193–209) (NeoMPS S.A., Strasbourg, France). After dilution in 0.1% TFA, the peptide fraction (10  $\mu\text{l}$ ) was trapped onto a C18 PepMap 100 (300- $\mu\text{m}$  inner diameter, 5 mm; Dionex) microprecolumn cartridge before the peptides were separated on a C18 PepMap column (75  $\mu\text{m}$ , inner diameter 150 mm; Dionex). Solvent A contained 2% acetonitrile, 0.08% formic acid, and 0.01% TFA in LC grade water, and solvent B contained 95% acetonitrile, 0.08% formic acid, and 0.01% TFA in LC grade water. The separation began with 5% solvent B for 5 min, and the concentration of solvent B was linearly increased from 5 to 50% over 60 min at a flow rate of 200 nl/min. The separated peptides were analyzed by ESI quadrupole TOF in positive ion mode. A voltage of 3 kV was applied to the nano-electrospray ion source (Proxeon Biosystems A/S, Odense, Denmark). MS and MS/MS data were acquired in continuum mode. Data-direct analysis was used to perform MS/MS analysis on 1+ to 3+ charged precursor ions. Spectra were collected in the selected mass range of 400–1500  $m/z$  for MS spectra and 60–2000  $m/z$  for MS/MS spectra. The mass spectrometer was operated in data-dependent mode using Analyst QS 1.1 software (Applied Biosystems, Framingham, MA) and automatically switched between MS and MS/MS acquisition when the intensity of the ions was above 10 counts per second. All data (MS and MS/MS) were submitted to MASCOT (version 2.2) to identify peptides. The search was performed against a home-made data base composed of 200 sequences of proteins from the common Repository of Adventitious Proteins (cRAP project; see the Global Proteome Machine Web site). A semitryptic enzymatic cleavage with five possible missed cleavages was used, and the peptide mass tolerance was set to 0.2 Da for MS and 0.2 Da for MS/MS data. Two variable modifications were selected to allow for the oxidation of methionine residues and deamidation of asparagine and glutamine residues. For each peptide identified, a maximum  $p$  value of 0.001, which corresponds to an average MASCOT score of at least 39, was consid-

## Behavior of Dystrophin R11–15 with Membrane Models

ered to be the prerequisite for peptide validation with a high degree of confidence. Under these conditions, the false peptide discovery rate was found to be 1.35% for the three samples. The identified peptides were quantified in a label-free manner (26) using the peak height of the extracted ion chromatograms in the raw MS chromatograms ( $\pm 0.2$  atomic mass units) using Analyst QS 1.1. Intensity variation between peptides from different samples (free or liposome-complexed) was considered significant when the intensity changed by a factor of at least 1.5.

### Molecular Modeling

Individual residues were assigned to the “*a–g*” positions within the heptads proposed by Winder (13) in predicted coiled-coil repeats. The fold recognition program mGenTHREADER (27, 28) was run to detect the best templates for comparative modeling. The alignment proposed by mGenTHREADER is consistent with the pattern proposed by Winder *et al.* (13) and Kusunoki *et al.* (29) with respect to the heptad motifs conserved in the spectrin repeats. Secondary structure predictions were performed by PSIPRED (27), which incorporates four feed-forward neural networks that analyze the output obtained from PSI-BLAST (available from the NCBI, National Institutes of Health, Web site). Homology models of DYS R11–15 were built using the software MODELLER 9.7 (30). MODELLER is a program based on satisfaction of spatial restraints generated on the target sequence using alignment with the three-dimensional structure of the template. The loop modeling protocol of MODELLER 9.7 (31) was used to refine the loops of the selected model. Starting with a random conformation, 40 structures were built for each loop. The generated structures were assessed using MODELLER output as well as additional evaluations. The program PROCHECK was used to assess the stereochemical quality of the structures (32) and was supplemented by ProSA-WEB (33), the Web-based version of ProSA (34), by VERIFY3D (35), and by examination on a graphic display. The secondary structure of the models was analyzed and represented with PyMOL (DeLano Scientific). Hydrophobic and electrostatic potentials on the molecular surfaces were calculated using rTools (Kristian Rother) and the Adaptive Poisson-Boltzmann Solver (36) software package, respectively, implemented in PyMOL.

## RESULTS

### Protein Purification and Amphiphilic Properties

DYS R11–15 presents a unique band on SDS-PAGE and Coomassie Blue staining at the expected molecular mass of 59 kDa (Fig. 1B). The protein identification was further confirmed by tandem mass spectrometry. The monomeric state with a Stokes radius of 3.4 nm was confirmed by size exclusion chromatography (Fig. 1C). On representative negatively stained electron micrographs, DYS R11–15 appears as an elongated or slightly curved rod 25–30 nm in length (Fig. 1D). Purified DYS R1–3 and R20–24 rod domains were used as controls in this study and were generated as described previously (9). At the air/liquid interface, adsorption of DYS R11–15 was followed by surface pressure measurements while varying the subphase protein concentration over the range 0.1–1  $\mu\text{M}$ . At each protein concentration, the surface pressure increased to a stable value,

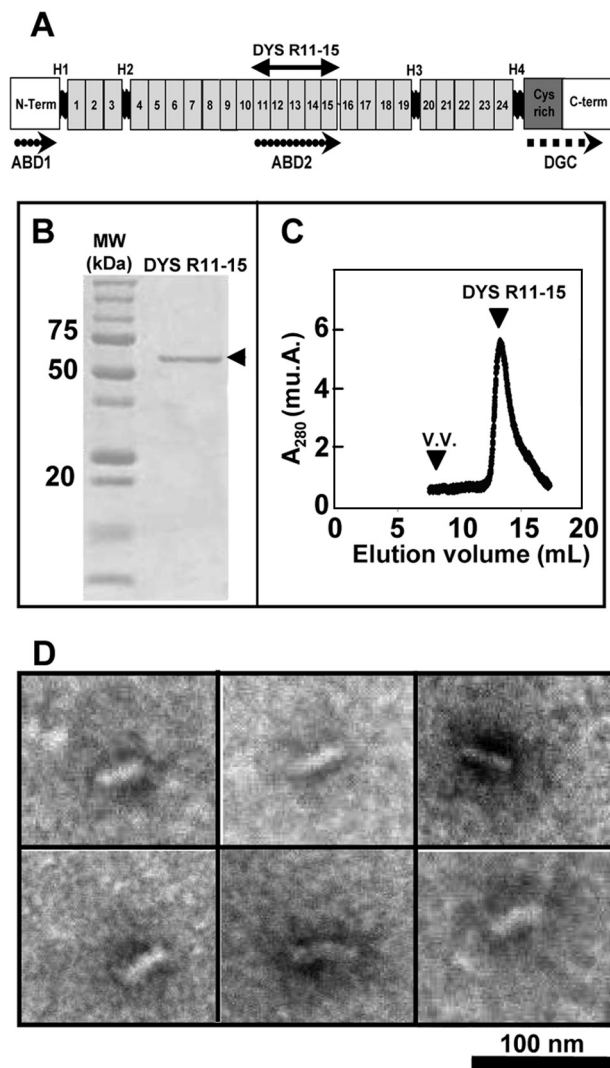


FIGURE 1. A, schematic illustration of the dystrophin protein. H1–H4, hinges 1–4; DGC, dystrophin-glycoprotein complex; ABD, actin binding domain; LBD, lipid binding domain as defined in Ref. 10. B, SDS-PAGE analysis of purified DYS R11–15 subdomain revealed by Coomassie Blue staining. DYS R11–15 is indicated by an arrow at 59 kDa. C, size exclusion chromatography of DYS R11–15. D, transmission electron micrographs of negatively stained DYS R11–15. V.V., void volume; *mu.A.*, milliunit of absorbance.

which indicated the end of the adsorption kinetics. This stable surface pressure increased with the protein concentration (Fig. 2A) up to a maximal value of 20.5 mN/m. At this surface pressure, the interface was saturated by protein regardless of the subphase concentration. The onset of this plateau was observed at a protein concentration of 0.1  $\mu\text{M}$ , and this concentration was therefore chosen for further experiments. To follow putative changes in the conformation of the protein at the air/liquid interface, PM-IRRAS spectra were acquired 20 h after protein injection at a bulk concentration of 0.1  $\mu\text{M}$  and a surface pressure of 20.5 mN/m. The spectra (Fig. 2B) contained one band located between 1700 and 1600  $\text{cm}^{-1}$  (centered at 1655  $\text{cm}^{-1}$ ) and another between 1600 and 1500  $\text{cm}^{-1}$  (centered at 1541  $\text{cm}^{-1}$ ). These bands attributed to the amide I and amide II signals, respectively (37), are characteristic of an  $\alpha$ -helical structure (38, 39). Therefore, the protein maintained its  $\alpha$ -helical structure at the interface. SDS-PAGE analysis indicated that no proteolysis had occurred (not shown).

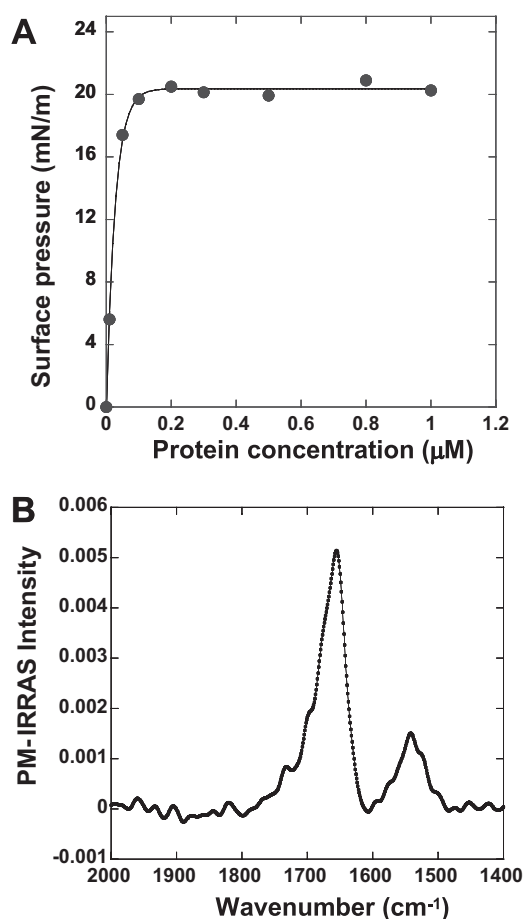


FIGURE 2. **Absorption of protein at the air/liquid interface.** *A*, the final surface pressure for different subphase concentrations reached at the end of kinetic adsorption. Each point corresponds to the mean value of three kinetic experiments. *B*, PM-IRRAS spectra acquired after protein adsorption at the air/liquid interface of DYS R11–15 (overnight after injection). The protein concentration in the subphase was  $0.1 \mu\text{M}$ .

In conclusion, the protein is adsorbed at the air/liquid interface while remaining in a stable and folded state after overnight adsorption, which demonstrates a strong amphiphilic character. This allowed for further experiments at the lipid/liquid interface.

#### DYS R11–15 and Liposome Interaction

When the anionic SUV (30 nm) concentration was increased, the fluorescence emission of tryptophan increased and reached a plateau. In contrast, DYS R11–15 tryptophan fluorescence progressively decreased in the presence of anionic LUVs of 100, 200, and 400 nm in diameter (Fig. 3A) and also decreased in the same manner in the presence of zwitterionic SUVs and LUVs of various diameters (Fig. 3B).

#### DYS R11–15 and Monolayer Interaction

*Interaction of DYS R11–15 with DOPC/DOPS and DOPC/DOPE Monolayers*—The binding between DYS R11–15 and anionic SUVs is well established; however, it appeared that binding was weak with anionic LUVs or with zwitterionic SUVs and LUVs. The contrast in binding properties between SUVs and LUVs could be accounted for by differences in curvature, whereas the contrast in binding with anionic *versus* zwitteri-

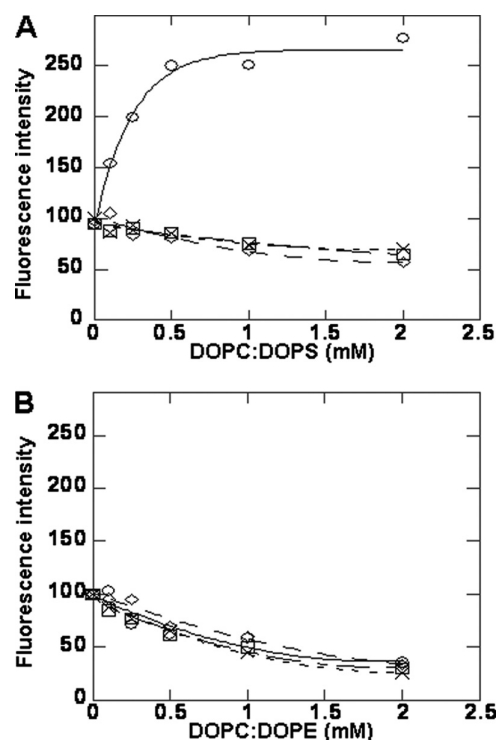


FIGURE 3. **Tryptophan fluorescence intensity of DYS R11–15 ( $0.5 \mu\text{M}$ ) following 2 h of incubation in the presence of different concentrations of lipid vesicles with DOPC/DOPS (A) and with DOPC/DOPE (B).** Lipid vesicle diameters were as follows: 30 nm ( $\circ$ ), 100 nm ( $\square$ ), 200 nm ( $\diamond$ ), and 400 nm ( $\times$ ).

onic SUVs is accounted for by differences in charges. Combining both low curvature and zwitterionic lipids might induce even weaker binding. Because it is known that the surface pressure of a monolayer can induce different binding properties for amphiphilic proteins by favoring electrostatic and hydrophobic forces, we examined the adsorption of DYS R11–15 to phospholipid anionic and zwitterionic monolayers at various initial surface pressures ( $\pi_i$ ). Both the DOPC/DOPE and DOPC/DOPS mixtures contained unsaturated hydrocarbon chains, so the pressure-area isotherms at the air/liquid interface are typical of a single liquid-expanded phase.

For all lipid compositions and initial surface pressures below a critical value ( $\pi_c$ ) discussed below, the pressure-area isotherms exhibited variations in both the surface pressure, ( $\Delta\pi = \pi_{\text{max}} - \pi_i$ ) (Fig. 4A) and the ellipsometric angle ( $\delta\Delta = \Delta_{\text{final}} - \Delta_{\text{lipid}}$ ) (Fig. 4B) due to the adsorption of DYS R11–15 to the lipid monolayer, which indicated that DYS R11–15 bound to both lipid mixtures. Such curves are classically drawn to analyze lipid-protein interaction and to highlight electrostatic and hydrophobic interactions (16–18, 40, 41).

These variations ( $\Delta\pi$  and  $\delta\Delta$ ) were greater at lower initial pressures (40). As  $\pi_i$  was increased, a critical surface pressure was achieved ( $\pi_c$ ), after which no further modification of the ellipsometric angle and overpressure were observed. These results indicated that no more protein could penetrate the monolayer. Thus, more DYS R11–15 can be inserted into the monolayer if the film is less condensed. However,  $\pi_i$  did exhibit some differences in its behavior in the two different lipid mixtures. Below  $\pi_i \sim 22.5 \text{ mN/m}$ ,  $\Delta\pi$  and  $\delta\Delta$  varied slightly

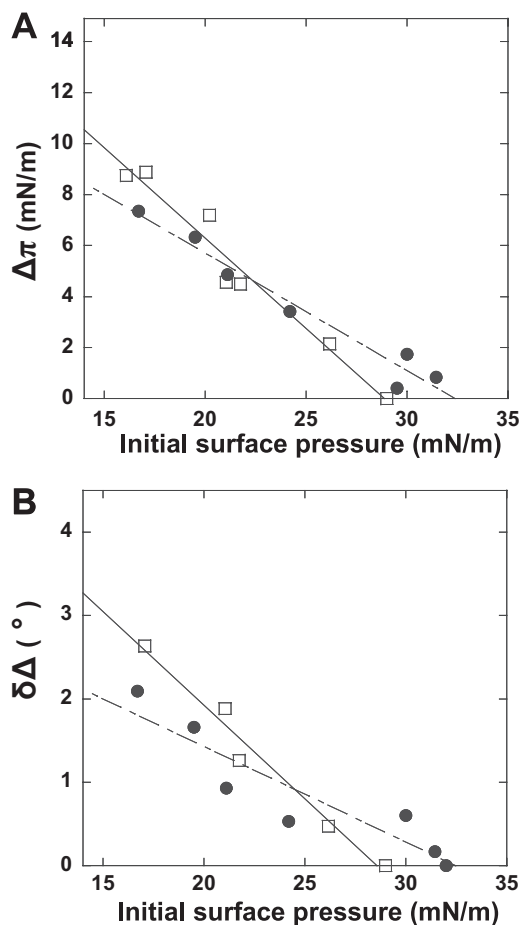


FIGURE 4. Increase of the surface pressure  $\Delta\pi$  (A) and of the ellipsometric angle  $\delta\Delta$  (B) at the end of the kinetic absorption of DYS R11–15 in phospholipid films versus the initial surface pressure ( $\pi_i$ ) of the monolayers of DOPC/DOPS (●) and DOPC/DOPE (□). The subphase concentration of R11–15 was  $0.1 \mu\text{M}$ . The measured critical surface pressures were 32 and 29 mN/m for the anionic and zwitterionic monolayers, respectively ( $T = 19^\circ\text{C}$ ; subphase, TNE buffer).

more in DOPC/DOPE than in DOPC/DOPS. Above  $\pi_i \sim 22.5$  mN/m, the opposite behavior was observed. The critical surface pressures were 32 and 29 mN/m for DOPC/DOPS and DOPC/DOPE, respectively. These differences show that, at lipid surface pressures below 22.5 mN/m, the binding of DYS R11–15 to lipid monolayers depends on the accessibility of hydrophobic zones, which dominate the DOPC/DOPE film. At surface pressures above 22.5 mN/m, binding is driven mostly by electrostatic forces, which dominate the DOPC/DOPS film. Therefore, DYS R11–15 inserts into less condensed films of zwitterionic lipids and into condensed films of anionic lipids.

In the presence of lipid monolayers and at a surface pressure of 20 mN/m, the variation of the overpressure versus DYS R11–15 concentration was measured with both lipid mixtures. We noticed that, in both cases, identical saturation concentrations ( $0.1 \mu\text{M}$ ) were determined with anionic (DOPC/DOPS) and zwitterionic (DOPC/DOPE) lipids (supplemental Fig. S1). These values are the same as those observed for saturation of the air/liquid interface by DYS R11–15, as shown in Fig. 2A. It appears that the saturation does not require higher concentrations when changing the lipid mixtures.

**DYS R11–15 Organization Depends on Lipid Packing**—To study the organization and to understand the evolution of the layer structure at the interface, AFM was used to image DYS R11–15 inserted into phospholipid layers at the mesoscopic scale. Results are displayed at initial surface pressures of 16, 20, and  $(\pi_c - 2)$  mN/m (i.e. 27 and 30 mN/m for DOPC/DOPE and DOPC/DOPS, respectively). These values were chosen because they are representative of significant changes in the organization of DYS R11–15. AFM images of the pure protein show a protein monolayer corresponding to the dark background, with some brighter spots formed by protein aggregation (Fig. 5G). Comparison of the AFM images of a pure lipid film (Fig. 5G, inset) and mixed phospholipid/protein films (Fig. 5, A–F) allows the bright protrusions (1.8–2.5 nm) to be attributed to the presence of proteins or protein-lipid complexes embedded in a darker matrix corresponding to the lipid monolayer. Images of DYS R11–15·DOPC/DOPS at  $\pi_i$  of 16 mN/m (Fig. 5A) show a heterogeneous distribution of protein or lipid/protein clusters with filament aggregation, whereas a network is observed at  $\pi_i$  of 20 and  $(\pi_c - 2)$  mN/m (Figs. 5, B and C). With DOPC/DOPE at  $\pi_i$  of 16 mN/m, DYS R11–15 is locally organized into interconnected clusters (Fig. 5D). At the initial surface pressures of 20 and  $(\pi_c - 2)$  mN/m, complete networks are observed (Fig. 6, E and F). The height ( $H$ ) and the width ( $W$ ) of the ridges that form the networks observed at 20 mN/m are significantly larger for DOPC/DOPE ( $H = 1.95$  nm,  $W = 78$  nm) than for DOPC/DOPS ( $H = 1.16$  nm,  $W = 58$  nm). At  $(\pi_c - 2)$  mN/m, the network height is quite similar in both lipid mixtures ( $\sim 1.8$  nm), whereas the network width in the anionic monolayer ( $\sim 58$  nm) is larger than that in the zwitterionic monolayer (39 nm). In agreement with the preceding data, which show that a low initial surface pressure favors protein insertion into DOPC/DOPE over DOPC/DOPS, the protein appears to be present in greater amounts in the AFM images of DOPC/DOPE than those of DOPC/DOPS. Moreover, the zwitterionic lipids induce organization of the protein molecules that leads to the beginning of a network, whereas in anionic lipid films, the proteins stay in individual clusters. By increasing the surface pressure, a network appears regardless the lipid nature. Nevertheless, a fine characterization of networks highlights little differences. Such behavior suggests that lipid/protein interactions induce molecular orientation changes and modulate protein/protein interactions depending on both the lipid type (anionic or not) and the lipid packing (initial surface pressure).

Because a similar protein network was observed at an initial surface pressure of 20 mN/m, we wondered whether the conformation of the protein was the same in the two cases. To investigate this possibility, the trypsin was injected into the subphase, and an Langmuir-Blodgett transfer was performed. After 20 min of proteolysis, a non-connected network remained in the DYS R11–15·DOPC/DOPS (Fig. 6A) sample. In contrast, the network in the DYS R11–15·DOPC/DOPS sample was nearly completely digested, and only a few protein clusters remained (Fig. 6C). After 2 h of trypsin digestion, both networks were entirely digested (Fig. 6, B and D). These results show that the network is primarily composed of DYS R11–15 and that trypsin accessibility to the protein is higher in the presence of zwitterionic lipids than in the presence of an anionic lipid.

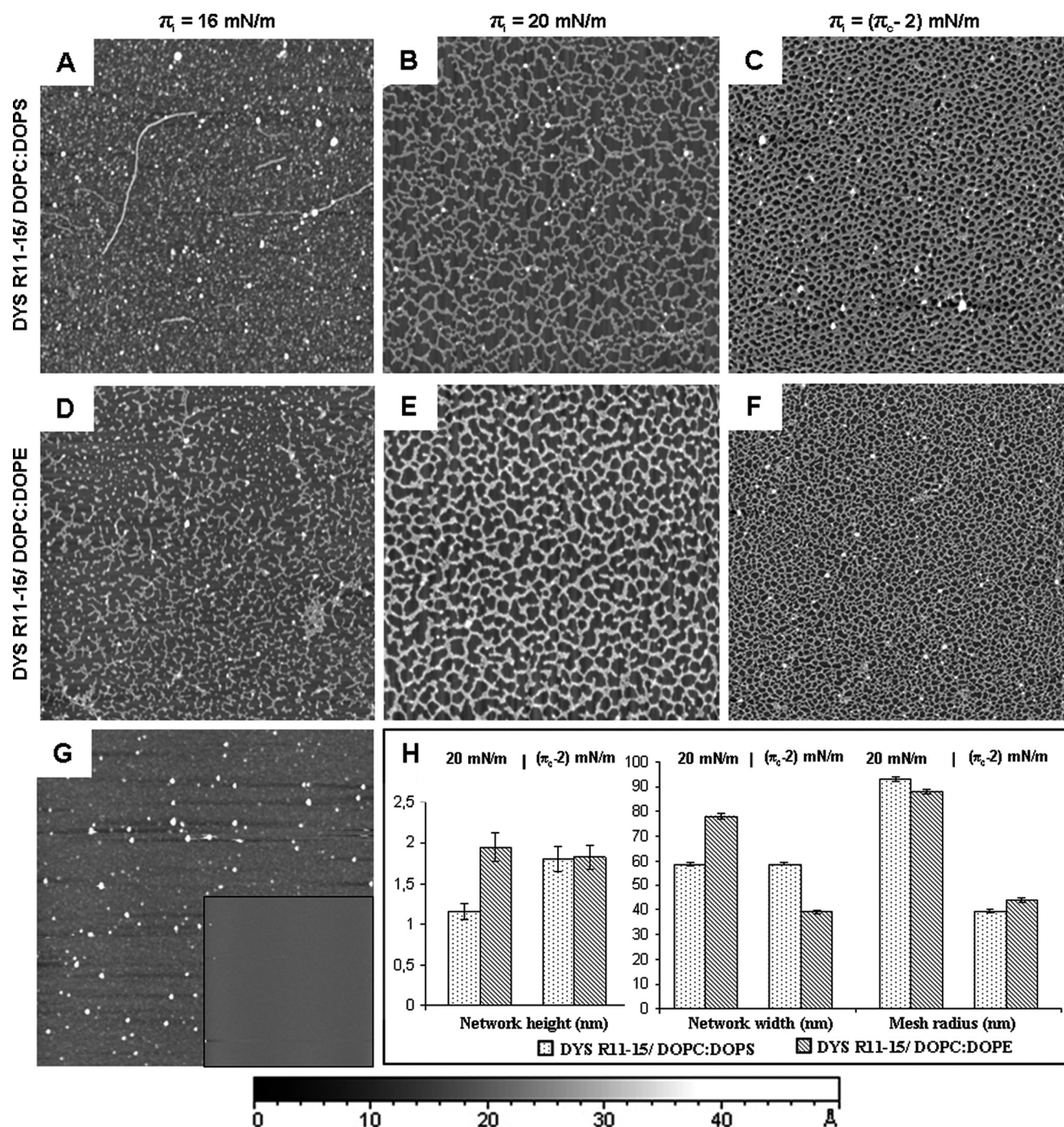


FIGURE 5. **AFM topographic images of transferred monolayers.** A–F correspond to the transferred protein/lipid films for protein adsorption onto the lipid monolayer at initial surface pressures of 16 mN/m (A and D), 20 mN/m (B and E),  $(\pi_c - 2)$  mN/m (C and F) using DOPC/DOPS (A–C) and DOPC/DOPE (D–F) as the lipid mixtures. G corresponds to DYS R11–15 at the air/liquid interface, and the inset represents the lipid monolayer DOPC/DOPS at 20 mN/m. In all images, the scan size is  $5 \times 5 \mu\text{m}$ , and the height scale is 5 nm. The histogram (H) presents the statistical analysis of the AFM images in B, C, E, and F (for details, see supplemental material).

onic monolayer. This difference in accessibilities strongly suggests that the conformation of DYS R11–15 is dependent on the nature of the lipid monolayer and that different regions of the protein may be involved in binding to the two distinct lipids. Therefore, it is of great interest to map the interacting regions. However, obtaining reliable detailed information at the molecular level from proteins processed under a monolayer in a Langmuir trough is quite difficult. Therefore, we chose to investigate the effects of proteolysis on DYS R11–15 using the vesicle model.

#### DYS R11–15 Proteolysis Patterns

Trypsin proteolysis of the protein and protein/vesicle mixtures was followed by SDS-PAGE (supplemental Fig. S2). When alone or in contact with DOPC/DOPS LUVs, the 59-kDa signal of full-length DYS R11–15 disappears after 20 min of digestion. In contrast, the signal disappears after only 5 min when the protein is in contact with DOPC/DOPS SUVs. A specific proteolysis product appears at 23 kDa when trypsin acts on DYS

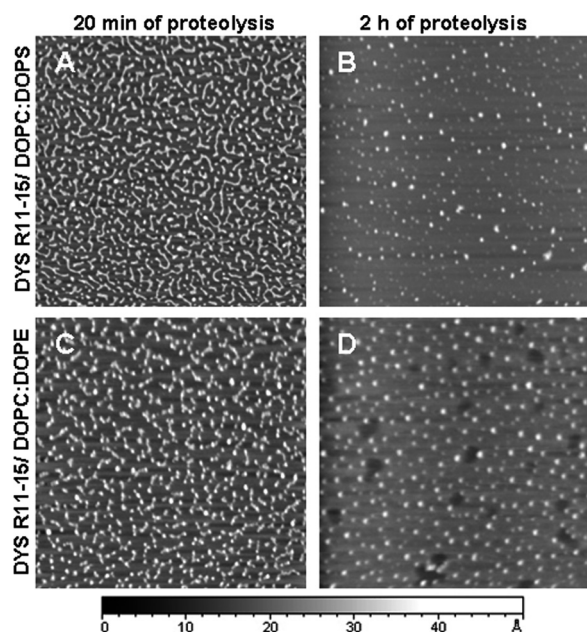


FIGURE 6. AFM topographic images of transferred monolayers after trypsin proteolysis. A–D, organization of DYS R11–15 in DOPC/DOPS (A and B) and DOPC/DOPE (C and D) monolayers at 20 mN/m after 20 min (A and C) or 2 h (B and D) of trypsin digestion. In all images, the scan size is  $5 \times 5 \mu\text{m}$ , and the height scale is 5 nm.

R11–15 that is bound to DOPC/DOPS SUVs. No significant changes in the proteolysis patterns were observed in SDS-PAGE when DOPC/DOPE SUVs or LUVs were mixed with the protein. The most significant differences between free DYS R11–15 and the lipid-protein complexes were observed when the protein was in contact with anionic SUVs. We focused label-free quantitative proteomics on trypsinized DYS R11–15 in the absence or presence of SUVs. We used biostatistical profiling (42) in which changes in the intensities of the peptide ions are recorded. MS/MS spectra allowed us to compare the ratios of the integrated peak areas/intensities of the peptide ions across samples (supplemental Fig. S4). The presence of the peptides that correspond to trypsin cleavage from residue 171 to residue 235 dramatically decreased when the protein was preincubated in the presence of DOPC/DOPS SUVs. The trypsin accessibility to the protein in this zone is reduced, which may be because DYS R11–15 interacts with lipid SUVs through this region or because the presence of the liposomes changes the conformation of the protein. Therefore, we named this region the zone protected from trypsin digestion in the presence of DOPC/DOPS SUVs, and this zone corresponds to residues 1632–1696 of full-length human dystrophin. When compared with trypsin action on the protein without any lipids, the intensity of the proteolytic peptides that ranged from residue 250 to residue 392 increased significantly when DYS R11–15 was preincubated in the presence of both DOPC/DOPS and DOPC/DOPE SUVs. These results reflect higher trypsin accessibility in the presence of liposomes, and this region was called the zone unprotected from trypsin digestion in the presence of SUVs and corresponds to residues 1711–1753 of full-length human dystrophin. The peptide intensities from residues 6–181 were slightly higher when DYS R11–15 was in the presence of the zwitterionic SUVs (supplemental Fig. S3A) and slightly lower in

the presence of the anionic SUVs (supplemental Fig. S3B). The explanation for these data is that, when the DOPC/DOPS protected zone interacts with the anionic SUVs, the area formed by amino acids 6–181 are brought very close to the membrane and will be less suitable for proteolysis. This explanation also accounts for the increase in fluorescence intensity that was observed with anionic SUVs due to the proximity of two tryptophan residues, Trp<sup>128</sup> and Trp<sup>155</sup>, with the hydrophobic lipid tails. The intensity variations between the peptides of different samples (free or with SUVs) in the other protein zones did not meet our criteria for significance.

#### Modeling and Mapping the Interactions Resulting from MS/MS Data

As expected, mGenTHREADER revealed that the best templates for DYS R11–15 were spectrin repeat proteins, particularly repeats 14–16 of human spectrin (Protein Data Bank code 3edv) (43) and repeats 15–16 of the chicken brain spectrin (Protein Data Bank code 1u5p) (44). DYS R11–13 shares 10.6% sequence identity with 3edv, and DYS R14–15 shares 19.6% sequence identity with 1u5p. As previously described (29), despite a relatively low percentage of sequence identity, the structures of individual spectrin-like repeats are nearly identical and provide good models for comparative modeling. Supplemental Fig. S4 presents the sequence alignments of DYS R11–15 with Protein Data Bank entries 3edv and 1u5p. We used MODELLER to build the model of DYS R11–15, and more than 100 homology models were generated in this manner. The models with GA341 scores higher than 0.6 with the lowest target function and DOPE scores were evaluated with ProSA-WEB and VERIFY3D. For the representative results shown in Fig. 7, profiles indicate a high quality model with a ProSA global score of  $-8.84$  and a positive mean force potential from VERIFY3D. After minimization, the Ramachandran map shows 93.6% of the residues in the most favored regions, 6.4% in the allowed zones, and no residues in the forbidden zones (see supplemental material). On a ribbon plot of the protein (Fig. 7A (a)), each repeat is structured as a triple  $\alpha$ -helical conventional coiled-coil (helices A–C). The DYS R11–15 model shows that the repeats are connected by the last helix (HC) of one repeat in continuity with the first helix (HA) of the next repeat. According to the selected model, the “a” and “d” residues (13) in the heptads lie on the inward facing surfaces of the helices and form the hydrophobic interaction core among the three helices. Fig. 7A (b and c) presents the hydrophobic and electrostatic surface properties, respectively. As expected for a soluble protein, the molecular surface of DYS R11–15 is mainly hydrophilic. The electrostatic potential at the molecular surface shows a distribution of negative and positive charge on the molecule. An intense negative charge is observed mainly on the repeats R12 and R13 of DYS R11–15. Visualization of the zones protected and unprotected from trypsin digestion defined earlier from MS data were performed on the three-dimensional structure obtained from homology modeling. The DOPC/DOPS SUVs protected zone from trypsin digestion is formed by the distal part of HB, the entire HC of repeat 12, and the proximal part of HA of repeat 13, as shown in red (Fig. 7B). The zone unprotected from trypsin digestion, formed by HB and HC of repeat

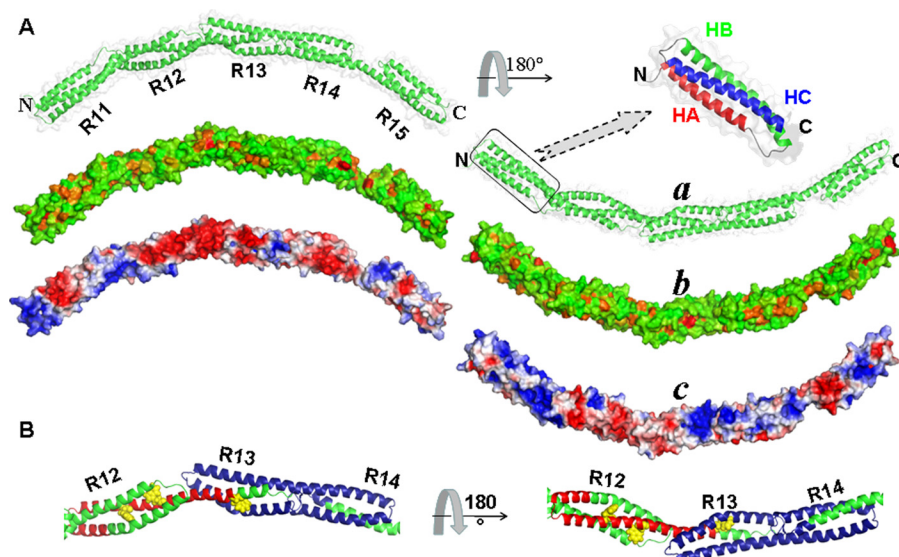


FIGURE 7. **Molecular modeling of DYS R11–15.** A, PyMOL representation of DYS R11–15 global fold (*a*). N and C termini are indicated as well as the repeat numbers of the central rod domain (R11–R15). Zooming in on repeat 11 of DYS R11–15 shows the triple coiled-coil helix formed by helices A, B, and C. The hydrophobic potential at the molecular surface (*b*) is colored by increasing hydrophobicity from green to red. The electrostatic potential at the molecular surface (*c*) is colored by increasing electrostatic potentials from red to blue. B, PyMOL representation of DYS R11–15 after peptide quantification using the MS/MS label-free technique. In red, the DOPC/DOPS protected zone (HB and HC of R12 and HA of R13) from trypsin digestion is shown, and in blue, the unprotected zone from trypsin digestion in the presence of lipids is shown (DOPC/DOPS or DOPC/DOPE). The tryptophan residues are shown in yellow.

13 and HA and HB of repeat 14, is shown in blue. Of the seven tryptophan residues in DYS R11–15, Trp<sup>202</sup> and Trp<sup>212</sup> on HC of R12 are in the DOPC/DOPS protected zone (shown in yellow), and the environment of Trp<sup>236</sup> is probably exposed to changes in the protected zone.

## DISCUSSION

In this study, we focused on the behavior of the central domain repeats (repeats 11–15) of dystrophin. Using two experimental membrane models, vesicles and monolayers, we demonstrated that the binding of DYS R11–15 to lipids is dependent on membrane curvature and lipid packing. We used recombinant DYS R11–15 protein that had been previously shown to exhibit 71%  $\alpha$ -helical content in solution and is considered to be properly folded (10). Our first observation was that DYS R11–15 displays an amphiphilic character and maintains its secondary helical structure at the interface. Similar conclusions have been reported for the DYS R2 single repeat and the DYS R1–3 multirepeat protein (8, 45).

We further investigated the interaction of DYS R11–15 with lipids. Steady-state fluorescence data demonstrated that the binding of DYS R11–15 was stronger to anionic than to zwitterionic SUVs or to either type of LUVs. However, when using lipid monolayers, it was determined that the mode and strength of the DYS R11–15 interaction with lipids depend more on the lipid nature and on the initial surface pressure of the monolayer. DYS R11–15 interacts more with the zwitterionic lipids than with the anionic monolayer when the initial surface pressure is less than 22.5 mN/m, because the headgroup of the DOPE phospholipid is smaller than that of DOPS. In addition, the hydrophobic tail is more accessible to the protein when the electrostatic contribution is very low or negligible. Conversely, when  $\pi_i$  is higher than 22.5 mN/m, DYS R11–15 has more affinity to the anionic monolayer, which is probably due to elec-

trostatic effects. Therefore, the critical surface pressure ( $\pi_c = 32$  mN/m) was slightly higher than that of DOPC/DOPE ( $\pi_c = 29$  mN/m). The interactions between DYS R11–15 and lipids are dependent on several factors, such as hydrophobic interactions, steric hindrance, and electrostatic attractions (46).

AFM image analyses show that the initial surface pressure of the lipids affects the organization of DYS R11–15 regardless of lipid composition. The formation of this network is a characteristic behavior of DYS R11–15, whereas DYS R1–3 and DYS R20–24 do not form networks under the same conditions (8). Although the lipids remain in a liquid-expanded state, the organization of DYS R11–15 is completely different at  $\pi_i = 16$  or 20 mN/m and with anionic or zwitterionic lipid mixtures. At an initial surface pressure of 16 mN/m, the less compact lipids promote partial insertion of DYS R11–15 into the lipid film, which is associated with a hydrophobic interaction, and the protein spreads over the lipid film. DYS R11–15 starts to organize into interconnected clusters with DOPC/DOPE at  $\pi_i = 16$  mN/m and generate a complete and well defined network at 20 mN/m. The same network was observed with DOPC/DOPS. Therefore, formation of the protein network through specific protein-protein interactions was promoted by the lipid monolayer and is due to the interfacial orientation of the proteins, which is observed at a lower pressure with DOPC/DOPE than with DOPC/DOPS. The headgroups of DOPC/DOPS are larger and more mobile than those of DOPC/DOPE, making DOPC/DOPS a more dynamic monolayer, and the hydrophobic tails of DOPC/DOPS are less accessible than those of the zwitterionic mixture. When the initial surface pressure ( $\pi_i = 20$  mN/m) increases, the film fluidity decreases and favors interfacial stabilization, orientation, and finally protein-protein interactions. In this case, the nature of the lipids does not play the major role. This result is in accordance with the same behavior observed in

## Behavior of Dystrophin R11–15 with Membrane Models

tryptophan fluorescence data of anionic and zwitterionic LUVs. DYS R11–15 is a monomer in solution and forms a protein monolayer with protein clusters at the air/liquid interface. We showed that the presence of a lipid monolayer induces protein-protein interactions, which do not form a random network but reflect a specific orientation of the protein. The results indicate that the dominant effects on protein organization are due to lipid packing rather than the charge and size of lipid heads. Nevertheless, the statistical characterization of the network at 20 mN/m shows differences on the protein network suggesting that a different and specific anchoring of the protein occurs with both lipid mixtures.

To better characterize the network and the orientation of the proteins under the monolayer, we used trypsin proteolysis in the subphase of a Langmuir trough. To our knowledge, this was the first time that trypsin accessibility assays were used under these conditions. The proteolysis patterns of DYS R11–15 under DOPC/DOPE and DOPC/DOPS monolayers are different after 20 min of trypsin action. Because the initial pressures were identical for both lipid mixtures, the results obtained by this approach confirm the conclusion that the molecular anchoring of DYS R11–15 beneath the monolayer depends on the nature of the lipid, whereas its organization depends on lipid packing.

No experimental x-ray or NMR structures are available for any of the dystrophin rod domain repeats. To date, only homology-based models have been proposed for single or several repeats of dystrophin (47, 48). We built a homology model of the three-dimensional structure of DYS R11–15 to gain insight into new structural information about the dystrophin rod domain and its binding to lipids. Interestingly, the five-repeat construct exhibits a regularly curved organization. Although unexpected, this *in silico* observation is compatible with transmission electron microscopy negative staining of the monomeric DYS R11–15 protein, which exhibited abundant curved forms with a mean length of 30 nm. Previous transmission electron microscopy studies on whole dystrophin also observed a long and relatively flexible rod-shaped molecule (49). Investigations of the biological significance of the flexibility of DYS R11–15 are in progress.

The three-dimensional structural model was used to interpret fluorescence data and label-free mass spectroscopy data with the aim of mapping the parts of the protein that interact with SUVs. The present study provides a detailed comparative analysis of the accessibility of lysine and arginine residues free and in SUV·DYS R11–15 complexes. The nano-LC/MS/MS allowed us to determine the protein interaction zone, which should be closely related to the changes in the fluorescence data. Interestingly, we were able to discriminate DOPC/DOPS and DOPC/DOPE specificity at the protein lipid interface on SUVs. We identified an area protected from trypsin action, one part of repeat R12 (HB and HC) and repeat R13 (HA), which is probably in contact with the lipid layer. Nevertheless, upon lipid binding, structural rearrangements within helix-helix interactions by moving heptads and rearrangements of hydrophobic residues in contact with lipids are likely to occur. This remark is in agreement with our previous circular dichroism analyses, which demonstrated that the protein remains structured in  $\alpha$ -helix when it interacts with DOPC/DOPS SUVs (10).

Three tryptophan residues are in the DOPC/DOPS protected zone, and no tryptophan residues are present in R11 and R14. Upon lipid binding to DOPC/DOPS SUVs, the fluorescence signal of DYS R11–15 changes because of changes in the environment of the tryptophan residues (Trp<sup>202</sup>, Trp<sup>212</sup>, and Trp<sup>236</sup>) located in R12 and R13. One particular target is amphiphilic helix C in repeat R12, which has two tryptophan residues (Trp<sup>202</sup> and Trp<sup>212</sup>). Penetration of these residues into the hydrophobic core of the liposome could explain the degree of variation in the fluorescence intensity when the protein binds to anionic SUVs. Moreover, we identified a region (HB-HC of R13 and HA-HB of R14) common to zwitterionic and anionic SUV binding where trypsin accessibility is higher than that of the protein in solution. Surprisingly, R13 is involved in protected and unprotected zones, so the binding to SUVs is probably due to R13, regardless of the lipid composition. In the three-dimensional model, the DOPC/DOPS protected areas exhibit a negative electropotential that, if the triple-coiled coil remains folded, would not be fully compatible with a strong interaction with negatively charged SUVs. Thus, in DOPC/DOPS SUVs, R13 binding would induce new folding interactions that would lead to favorable electrostatic and hydrophobic interactions and increase the stability of the DYS R11–15 DOPC/DOPS SUV complex. In addition, because the fluorescence signals were identical for DOPC/DOPE SUVs and LUVs, it is tempting to postulate that the binding or destabilizing interaction with R13 may also appear with DOPC/DOPE LUVs. These results corroborate the above conclusions that the protein is more influenced by packing than by the lipid nature in SUVs, where the balance between hydrophobic and hydrophilic zones is very different due to the geometric lipid shapes (50). Moreover, the highly curved bilayers exhibit defects in lipid packing, and the amphipathic helices can insert as hydrophobic wedges (51). The ability of DYS R11–15 to bind lipids could be a result of a helix insertion being facilitated by a transient low density region.

Taken together, the present data concerning the behavior of DYS R11–15 in the presence of vesicles (SUVs/LUVs) and under monolayers lead to interesting conclusions. It is striking that the sarcolemma ruptures very frequently (52) in dystrophin-deficient muscles. In normal muscles, packing of lipids and the curvature of membrane blebs may vary according to the muscular status during contraction (high surface pressure) or extension (low surface pressure). Little is known about full-length dystrophin self-organization in living cells, except that its presence as subsarcolemmal orthogonal arrays has been revealed by immunofluorescence (53). There is clear evidence that dystrophin is involved in the resistance of sarcolemmal membranes to stress induced by the contraction-relaxation cycles of active muscles. Our study demonstrates that the DYS R11–15 subdomain of the dystrophin rod plays a central role in membrane resistance through interactions with lipid bilayers at different curvatures. The proteins insert into the lipid layer at low lipid packing through hydrophobic forces, and under higher lipid packing, they are tightly attached to the lipids through electrostatic forces. We showed that the helical structure is maintained, and the protein organization is modified by the lateral pressure of the associated lipids. In cellular conditions, events in which some parts of the rod domain

bind more strongly when lipid packing is high could stabilize blebs or membrane reservoirs; our present findings reflect a physiologically adaptive process. Therefore, the dystrophin DYS R11–15 could provide the phospholipid membrane with the solid support essential to maintaining membrane cohesion (54, 55). In support of this role for DYS R11–15 binding to membrane lipids, it is worth mentioning that truncated dystrophin that lacks this region is less efficient at rescuing the normal phenotype of the dystrophin-deficient mdx mouse (6, 56).

Finally, DYS R11–15 is known as the actin-binding domain ABD2. Data from the present work show that DYS R12 and R13 bind lipids. Because the actin-binding domain of DYS R11–15 is not precisely mapped, one exciting question concerns the possibility that both sarcolemma and actin filaments simultaneously bind to dystrophin through the DYS R11–15 region.

*Acknowledgments*—We thank Christophe Tascon, Agnès Burel, and the IFR 140 Microscopy Department for technical support.

## REFERENCES

- Koenig, M., Hoffman, E. P., Bertelson, C. J., Monaco, A. P., Feener, C., and Kunkel, L. M. (1987) *Cell* **50**, 509–517
- Ervasti, J. M., Kahl, S. D., and Campbell, K. P. (1991) *J. Biol. Chem.* **266**, 9161–9165
- Campbell, K. P., and Kahl, S. D. (1989) *Nature* **338**, 259–262
- Amann, K. J., Renley, B. A., and Ervasti, J. M. (1998) *J. Biol. Chem.* **273**, 28419–28423
- Deconinck, N., and Dan, B. (2007) *Pediatr. Neurol.* **36**, 1–7
- Harper, S. Q., Hauser, M. A., DelloRusso, C., Duan, D., Crawford, R. W., Phelps, S. F., Harper, H. A., Robinson, A. S., Engelhardt, J. F., Brooks, S. V., and Chamberlain, J. S. (2002) *Nat. Med.* **8**, 253–261
- Le Rumeur, E., Winder, S. J., and Hubert, J. F. (2010) *Biochim. Biophys. Acta* **1804**, 1713–1722
- Vié, V., Legardinier, S., Chieze, L., Le Bihan, O., Qin, Y., Sarkis, J., Hubert, J. F., Renault, A., Desbat, B., and Le Rumeur, E. (2010) *Biochim. Biophys. Acta* **1798**, 1503–1511
- Legardinier, S., Hubert, J. F., Le Bihan, O., Tascon, C., Rocher, C., Raguénès-Nicol, C., Bondon, A., Hardy, S., and Le Rumeur, E. (2008) *Biochim. Biophys. Acta* **1784**, 672–682
- Legardinier, S., Raguénès-Nicol, C., Tascon, C., Rocher, C., Hardy, S., Hubert, J. F., and Le Rumeur, E. (2009) *J. Mol. Biol.* **389**, 546–558
- Manno, S., Takakuwa, Y., and Mohandas, N. (2002) *Proc. Natl. Acad. Sci. U.S.A.* **99**, 1943–1948
- Fiehn, W., Peter, J. B., Mead, J. F., and Gan-Elepano, M. (1971) *J. Biol. Chem.* **246**, 5617–5620
- Winder, S. J., Gibson, T. J., and Kendrick-Jones, J. (1995) *FEBS Lett.* **369**, 27–33
- Laemmli, U. K. (1970) *Nature* **227**, 680–685
- Le Rumeur, E., Fichou, Y., Pottier, S., Gaboriau, F., Rondeau-Mouro, C., Vincent, M., Gally, J., and Bondon, A. (2003) *J. Biol. Chem.* **278**, 5993–6001
- Larios, C., Miñones, J., Jr., Haro, I., Alsina, M. A., Busquets, M. A., and Trillo, J. M. (2006) *J. Phys. Chem. B* **110**, 23292–23299
- Vié, V., Van Mau, N., Pomarède, P., Dance, C., Schwartz, J. L., Laprade, R., Frutos, R., Rang, C., Masson, L., Heitz, F., and Le Grimmelc, C. (2001) *J. Membr. Biol.* **180**, 195–203
- Sospedra, P., Nagy, I. B., Haro, I., Mestres, C., Hudecz, F., and Reig, F. (1999) *Langmuir* **15**, 5111–5117
- Blaudez, D., J.-M. Turllet, Dufourcq, J., Bard, D., Buffeteau, T., and Desbat, B. (1996) *J. Chem. Soc. Faraday Trans.* **92**, 525–530
- Blaudez, D., Buffeteau, T., Cornut, J. C., Desbat, B., Escafre, N., Pézolet, M., and Turllet, J. M. (1993) *Appl. Spectrosc.* **47**, 869–874
- Brockman, H. (1999) *Curr. Opin. Struct. Biol.* **9**, 438–443
- Azzam, R. M. A., and Bashara, N. M. (1977) *Ellipsometry and Polarized Light*, p. 340, Elsevier/North Holland, Amsterdam
- Berge, B., and Renault, A. (1993) *Europhys. Lett.* **21**, 773–777
- Mikrut, J. M., Dutta, P., Ketterson, J. B., and MacDonald, R. C. (1993) *Phys. Rev. B* **48**, 14479
- Chi, L. F., Anders, M., Fuchs, H., Johnston, R. R., and Ringsdorf, H. (1993) *Science* **259**, 213–216
- Boutrou, R., Jardin, J., Blais, A., Tomé, D., and Léonil, J. (2008) *J. Agric. Food Chem.* **56**, 8166–8173
- Jones, D. T. (1999) *J. Mol. Biol.* **287**, 797–815
- McGuffin, L. J., Bryson, K., and Jones, D. T. (2000) *Bioinformatics* **16**, 404–405
- Kusunoki, H., MacDonald, R. I., and Mondragón, A. (2004) *Structure* **12**, 645–656
- Sali, A., and Blundell, T. L. (1993) *J. Mol. Biol.* **234**, 779–815
- Fiser, A., Do, R. K., and Sali, A. (2000) *Protein Sci.* **9**, 1753–1773
- Laskowski, R. A., Rullmann, J. A., MacArthur, M. W., Kaptein, R., and Thornton, J. M. (1996) *J. Biomol. NMR* **8**, 477–486
- Wiederstein, M., and Sippl, M. J. (2007) *Nucleic Acids Res.* **35**, W407–W410
- Sippl, M. J. (1993) *J. Comput. Aided Mol. Des.* **7**, 473–501
- Lüthy, R., Bowie, J. U., and Eisenberg, D. (1992) *Nature* **356**, 83–85
- Baker, R. D. (2001) *Lifetime Data Anal.* **7**, 65–83
- Jackson, M., and Mantsch, H. H. (1995) *Crit. Rev. Biochem. Mol. Biol.* **30**, 95–120
- Lavoie, H., Blaudez, D., Vaknin, D., Desbat, B., Ocko, B. M., and Salesse, C. (2002) *Biophys. J.* **83**, 3558–3569
- Bottier, C., Géan, J., Desbat, B., Renault, A., Marion, D., and Vié, V. (2008) *Langmuir* **24**, 10901–10909
- Chièze, L., Bolanos-Garcia, V. M., Pinot, M., Desbat, B., Renault, A., Beau-fils, S., and Vié, V. (2011) *J. Mol. Biol.* **410**, 60–76
- Pérez, J. A., Haro, I., Martín, I., Alsina, M. A., and Reig, F. (1995) *Anal. Chim. Acta* **303**, 65–72
- Kearney, P., and Thibault, P. (2003) *J. Bioinform. Comput. Biol.* **1**, 183–200
- Davis, L., Abdi, K., Machius, M., Brautigam, C., Tomchick, D. R., Bennett, V., and Michaely, P. (2009) *J. Biol. Chem.* **284**, 6982–6987
- Kusunoki, H., Minasov, G., Macdonald, R. I., and Mondragón, A. (2004) *J. Mol. Biol.* **344**, 495–511
- DeWolf, C., McCauley, P., Sikorski, A. F., Winlove, C. P., Bailey, A. I., Kahana, E., Pinder, J. C., and Gratzer, W. B. (1997) *Biophys. J.* **72**, 2599–2604
- Demel, R. A., Paltauf, F., and Hauser, H. (1987) *Biochemistry* **26**, 8659–8665
- Legardinier, S., Legrand, B., Raguénès-Nicol, C., Bondon, A., Hardy, S., Tascon, C., Le Rumeur, E., and Hubert, J. F. (2009) *J. Biol. Chem.* **284**, 8822–8832
- Krieger, C. C., Bhasin, N., Tewari, M., Brown, A. E., Safer, D., Sweeney, H. L., and Discher, D. E. (2010) *Cytoskeleton* **67**, 796–807
- Pons, F., Augier, N., Heilig, R., Léger, J., Mornet, D., and Léger, J. J. (1990) *Proc. Natl. Acad. Sci. U.S.A.* **87**, 7851–7855
- Israelachvili, J. N., Mitchell, D. J., and Ninham, B. W. (1977) *Biochim. Biophys. Acta* **470**, 185–201
- Hatzakis, N. S., Bhatia, V. K., Larsen, J., Madsen, K. L., Bolinger, P. Y., Kunding, A. H., Castillo, J., Gether, U., Hedegård, P., and Stamou, D. (2009) *Nat. Chem. Biol.* **5**, 835–841
- Petrof, B. J., Shrager, J. B., Stedman, H. H., Kelly, A. M., and Sweeney, H. L. (1993) *Proc. Natl. Acad. Sci. U.S.A.* **90**, 3710–3714
- Prins, K. W., Humston, J. L., Mehta, A., Tate, V., Ralston, E., and Ervasti, J. M. (2009) *J. Cell Biol.* **186**, 363–369
- Hamill, O. P., and Martinac, B. (2001) *Physiol. Rev.* **81**, 685–740
- Sheetz, M. P., Sable, J. E., and Döbereiner, H. G. (2006) *Annu. Rev. Biophys. Biomol. Struct.* **35**, 417–434
- Liu, M., Yue, Y., Harper, S. Q., Grange, R. W., Chamberlain, J. S., and Duan, D. (2005) *Mol. Ther.* **11**, 245–256
- Koenig, M., and Kunkel, L. M. (1990) *J. Biol. Chem.* **265**, 4560–4566

## **Spectrin-like Repeats 11–15 of Human Dystrophin Show Adaptations to a Lipidic Environment**

Joe Sarkis, Jean-François Hubert, Baptiste Legrand, Estelle Robert, Angélique Chéron, Julien Jardin, Eric Hitti, Elisabeth Le Rumeur and Véronique Vié

*J. Biol. Chem.* 2011, 286:30481-30491.

doi: 10.1074/jbc.M111.243881 originally published online June 28, 2011

---

Access the most updated version of this article at doi: [10.1074/jbc.M111.243881](https://doi.org/10.1074/jbc.M111.243881)

### Alerts:

- [When this article is cited](#)
- [When a correction for this article is posted](#)

[Click here](#) to choose from all of JBC's e-mail alerts

### Supplemental material:

<http://www.jbc.org/content/suppl/2011/06/29/M111.243881.DC1>

This article cites 56 references, 12 of which can be accessed free at <http://www.jbc.org/content/286/35/30481.full.html#ref-list-1>